Unified Kinetic Model of Dopant Segregation During Vapor-Phase Growth

Unified kinetic model of dopant segregation during vapor-phase growth

Craig B. Arnold[1,*] and Michael J. Aziz[2]
[1]*Department of Mechanical and Aerospace Engineering and Princeton Institute for Science and Technology of Materials, Princeton University, Princeton, New Jersey 08544, USA*
[2]*Division of Engineering and Applied Sciences, Harvard University, Cambridge, Massachusetts 02138, USA*
(Received 15 October 2004; revised manuscript received 6 September 2005; published 18 November 2005)

We develop a unified kinetic model for surface segregation during vapor phase growth that concisely and quantitatively describes the observed behavior in silicon-based systems. A simple analytic function for the segregation length is derived by treating terrace-mediated and step-edge-mediated mechanisms in parallel. The predicted behavior of this parameter is examined through its temperature, flux, and terrace length dependence. Six distinct temperature regimes are predicted for the segregation length that depend on the relative segregation energies and activation barriers of the two mechanisms. The model is compared to reported behavior of Sb and P in Si(001) and excellent agreement is obtained using realistic energies and preexponential factors. The model accounts for the experimentally observed anomalous low-temperature segregation of Sb as a consequence of the competition between step-edge-mediated segregation, dominant at low temperatures, and terrace-mediated segregation, dominant at higher temperatures. The generalized treatment of segregation mechanisms in the model makes it applicable to other segregating systems, including metals and III-V semiconductors.

DOI: 10.1103/PhysRevB.72.195419 PACS number(s): 68.35.Dv, 81.15.Aa, 68.55.Ln

I. INTRODUCTION

Recent advances in thin-film growth technology to improve density, speed, or other device properties require accurate control of impurities and dopants at small length scales. Complex architectures such as delta-doping[1,2] or band-gap engineering[3] for quantum well devices[4–6] or spintronic applications[7,8] require sharp heterostructures in semiconductors. Similarly, innovative metal-based structures such as giant magnetoresistive[9,10] or nanomagnetic devices[11,12] rely on the fabrication of abrupt interfaces. As the need for these sharp interfaces has become increasingly important, the problems of segregation, whereby one species of atom tends to preferentially move to the free surface during thin-film growth, remain a hindrance.

Growth of sharp interface structures is experimentally challenging but possible with well-controlled physical vapor deposition techniques such as pulsed deposition,[13,14] energetic techniques,[15] low-temperature molecular beam epitaxy (LT-MBE),[16] and surfactant mediated approaches.[17,18] Although one can achieve sharp jumps in composition, often a tradeoff must be struck between suppressed segregation and defect accumulation[19] so as to preclude the incorporation of an arbitrary concentration-depth profile.

Despite an abundance of experimental observations, there is no consensus on a physical mechanism underlying segregation and trapping. Any successful model for segregation must explain (1) the experimentally observed temperature dependence at low temperatures, (2) experimentally observed temperature dependence at high temperatures, and (3) the experimentally observed deposition rate dependence. Typically, in such segregating systems, the high-temperature regime is characterized by local equilibrium segregation, determined by the thermodynamic balance between the free energies of the surface and subsurface states.[20] In this regime, the amount of segregated material decreases as the temperature increases because more impurity is soluble in the host material. At lower temperature, the system is considered to be in a kinetically limited segregation regime. In this case, the segregation is determined by the kinetics of moving impurity atoms, and the relatively low mobilities cause them to become trapped in the growing film. As the temperature increases, the amount of segregated material increases because impurity atoms have enough mobility to move ahead of the growing film.

In this paper, an analytic model for segregation is developed that successfully describes the fundamental physics of the segregation phenomenon, yet is simple enough to enable easy comparison with experimental measurements without the need for numerical solutions or simulations. The development is based on earlier models of liquid phase growth[21,22] but with the introduction of multiple classes of exchange mechanisms for segregation at different sites on the growth surface. The model is developed in the context of segregation for dilute dopants in Si(001); however, the principles are sufficiently general that it can be applicable to other systems such as metallic alloys or III-V semiconductors. We demonstrate the effectiveness of the model by reproducing, for the first time, the measured temperature and growth rate dependence for Sb and P in Si(001).

II. BACKGROUND

There is a variety of models for surface segregation during thin film growth. For the purposes of our unified model, we classify them into three categories based on the mechanisms and approach to modeling. As these models have been discussed extensively in the literature, a detailed discussion of each is beyond the scope of this article.

A. Phenomenological

In this earliest class of segregation model, the overall process of segregation is discussed without kinetic details of the

atomic processes.[23–26] Rather, these models treat the flux of incorporated and segregated atoms at the surface in order to derive relations between the amount of segregation and the temperature. Given certain assumptions such as incorporation proportional to surface coverage[23] or exponentially varying diffusion near the surface,[27] phenomenological formulations show a transition between kinetically limited and equilibrium segregation that agrees qualitatively with experimental observations.

B. Terrace mediated

The first main modification to the phenomenological models included the introduction of atomic exchange between different layers in the growing film.[20,28] In these works, the individual layers in the structures are treated as flat and terrace-like with an unspecified kinetic pathway for exchange occurring between them. Exchange between two adjacent layers is allowed to proceed provided these are at the free surface. Deposition at discrete time intervals halts the exchange as a new surface layer is formed and another layer is buried in the bulk. Later incarnations of these models included the possibility of self-limiting behavior whereby impurity atoms in one layer exchange with impurity atoms in the adjacent layer, resulting in no increase of segregation.[29,30]

These terrace-mediated models have been shown to be sufficient in describing much of the physical behavior in the real systems. As with the phenomenological models, these models predict a transition between a kinetically limited low-temperature regime and an equilibrium regime at higher temperatures. However, the explicit introduction of an exchange mechanism enabled not only a better fit to experimental data, particularly at higher temperatures, but also enabled an experimental measurement of the energy barriers for this process.

C. Step-edge mediated

Two of the main shortcomings of the terrace-mediated models are that it neglects the presence of steps and roughness on the surface and it is insufficient to describe the experimentally measured behavior at low temperatures. To overcome these issues, models were developed to address the roughness of the surface and exchange of atoms at steps as a low-temperature mechanism to increase segregation.[31–33] Jesson *et al.* further demonstrated the importance of such mechanisms through experiments and calculations of Si-Ge growth in showing that it can be energetically favorable for atoms to climb at step edges.[34,35]

Significant differences exist among the step edge models in how segregation and incorporation are treated. Nonetheless, the introduction of low-temperature mechanisms enabled these models to improve the agreement with experiment in certain temperature regimes. However, in many cases, these models fell short in accurately predicting the transitions between kinetically limited and equilibrium segregation, or in predicting other experimental dependencies such as growth rate or surface miscut dependence.

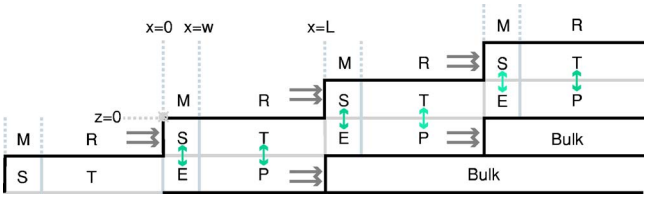

FIG. 1. (Color online) Simplified view of surface layers and exchanges. M: adatoms above step edge, R: adatoms above terrace, S: step edge, T: terrace, E: below step edge, P: below terrace. Single arrows denote locations of diffusive exchange, double arrows denote regions of convective flux. Bold lines in the figure denote no exchanges allowed across boundary, and the small circle denotes the origin for the coordinate system.

D. Summary of previous models

Although the individual models outlined in the above sections are not optimal for our development objectives, each class provides important physical understanding to the segregation phenomenon. Phenomenological models indicate a transition between two segregation regimes, terrace models describe high-temperature regimes, surface-mediated models describe low-temperature regimes, and simulations[36–38] enumerate kinetic pathways for segregating atoms. In developing a unified model we capitalize on the strengths of each model class.

III. THE MODEL

A. Segregation kinematics

The complexity of any given growth surface makes a rigorous kinetic treatment of all possible segregation mechanisms analytically untenable. Consequently we model the surface as a periodic structure, undergoing step-flow growth, where each period contains seven distinct structural regions, as shown in Fig. 1. The space between steps is divided into a step-edge region (M,S,E) of length w, and a terrace region (R,T,P) of length L-w. The monolayer spacing in the z direction is a and the surface is considered to be screw periodic with repeat vector $r=L\hat{x}+a\hat{z}$. The surface is uniform in the y direction, but for dimensional purposes, we define a_o as the lattice parameter of one conventional unit cell in the x and y directions. For an (001) surface $a_o=4a$. The origin of our coordinate system is fixed on the top of the moving step edge and we keep track of only the motion of impurity atoms.

Impurity ("B") atoms are allowed to move between the regions via direct interchange ("exchange") events between B atoms and host ("A") atoms with the condition that they are immobile in the bulk region. Our model is not concerned with the detailed kinetic pathway for a given exchange event, but rather the effective result of an impurity atom moving from one location to another. It should be noted that this method of simplifying the surface processes could be extended to include additional layers at the surface of the film, if necessary.

There are several metrics available to quantify the segregation behavior and the most appropriate choice depends on the experimental conditions. For example, in one class of

experiments the impurity and host species are deposited concurrently over the entire course of the experiment (codeposition). In this case a relevant measure for segregation is the Gibbsian surface excess. If there is negligible evaporation from the free surface, the system establishes a steady-state (positive or negative) surface excess of impurity with the composition of the bulk region fixed at the composition of the incident flux. If evaporation is significant, the system still establishes a steady-state surface excess, however the composition of the bulk region differs from that of the incident flux by a term proportional to the evaporation flux. By locating the Gibbsian dividing surface at the interface between the vapor phase and the substrate surface, the Gibbsian surface excess, Γ, is given by

$$\Gamma \equiv \frac{1}{a_o L}\int_{-\infty}^{0}\int_{0}^{a_o}\int_{0}^{L}[C(x,z)-C^{bulk}]dxdydz, \tag{1}$$

where C_{bulk} is the concentration of the steady-state bulk material and $C(x,z)$ is the concentration at location (x,z) in the surface.

We can refine this definition for our model by noting that the surface region, the region in which the impurity atoms are able to make exchanges, has only a finite depth, ζ. Beyond this depth the mobility is negligibly small, the composition must equal the bulk composition, and the above integrand vanishes. Therefore,

$$\Gamma = \frac{1}{L}\int_{-\zeta}^{0}\int_{0}^{L}C(x,z)dxdz - \zeta C^{bulk}. \tag{2}$$

One important consequence of Eq. (2) is that Γ can exceed one complete monolayer of impurity atoms. Such behavior has been experimentally observed in the case of Si and Ge,[39,40] but previous models were unable to account for this behavior.

A second class of experiments is characterized by serial deposition, in which the impurity atoms are deposited first, followed by subsequent deposition of host only. This type of experiment may be associated with "delta doping" or "surfactant-mediated" growth processes.[2,41] The surface impurity concentration decays over time as impurity atoms become trapped in the bulk or evaporate and are not replenished by a deposition flux. In this case a relevant measure of segregation is the segregation ratio r as defined by Jorke,[28]

$$r = \frac{\text{Areal concentration of impurity in the surface}}{\text{Volume concentration of impurity in the bulk}}. \tag{3}$$

This parameter has the units of length and is therefore sometimes referred to as the segregation length.

From Eq. (2) we can find the 2-D areal concentration of impurity in the surface region, $\langle n\rangle$, by integrating the concentration over all regions of the surface and dividing by the projected area in the x-y plane,[42]

$$\langle n\rangle = \frac{1}{a_o L}\int_{-\zeta}^{0}\int_{0}^{a_o}\int_{0}^{L}C(x,z)dxdydz. \tag{4}$$

We integrate this equation over the y dimension and divide by the bulk concentration to yield the equation for r,

$$r = \frac{1}{LC^{bulk}}\int_{-\zeta}^{0}\int_{0}^{L}C(x,z)dxdz. \tag{5}$$

The literature provides a variety of metrics to quantify the concentration profile under serial deposition experiments. However, these measures are related by appropriate transformations under particular conditions. For example, the partition coefficient,[30] which is defined as the bulk concentration normalized by the surface concentration, is simply the inverse of r multiplied by the monolayer spacing a. The profile broadening, Δ, defined as the $1/e$ decay length of the 2-D surface concentration vs distance grown, reduces to the segregation ratio [Eq. (3)] when evaporation is negligible.[28,32] In the case where evaporation cannot be ignored, one calculates the relationship between Δ and r by solving the equation relating surface concentration to the changing height of the surface,

$$\frac{d\langle n\rangle}{dz} = -\langle n\rangle\left(\frac{1}{r}+\frac{k^{evap}}{v_z}\right). \tag{6}$$

In this equation, k^{evap} is the evaporation rate constant, given by $\nu\exp(-E/k_BT)$, where ν is an effective vibration frequency and v_z is the velocity of growth in the z direction. The solution to the differential equation for $\langle n\rangle$ is recognized as an exponential with a $1/e$ decay length of

$$\Delta = \frac{1}{\left(\frac{1}{r}+\frac{k^{evap}}{v_z}\right)}. \tag{7}$$

The above equation goes to the appropriate limit of $\Delta \to r$ as k^{evap} goes to zero.

Although the codeposition and serial deposition experiments seem fundamentally different, Eqs. (2) and (5) show their measures of segregation are related by

$$r = \frac{\Gamma}{C^{bulk}} + \zeta. \tag{8}$$

Our model is developed from the steady-state co-deposition case described above. By finding a solution for Γ, one readily uses Eq. (8) to determine r for the non-steady-state case that describes the experimental results.[43] We apply our model to these experiments under the quasi-stationary assumption that the surface concentration profile equilibrates rapidly on the time scale of changes in Γ itself.

B. Kinetics

Define C^{α} as the concentration of B atoms in region α, $J^{\alpha\beta}$ as the vertical diffusive flux of B atoms from region α to region β, D^{α} as the lateral diffusivity of B atoms within region α, $k^{\alpha,evap}$ as the rate of evaporation from region α, v as the speed of the moving step edge with respect to the lattice, F as the projected deposition flux (atoms/site·s), and f as the fraction of incident B atoms in the deposition flux. Then in the moving reference frame centered on the step edge at $(x,z)=(0,0)$, the concentration at a particular location within each region evolves with time due to vertical

diffusion into and out of the region, lateral diffusion within the region, and a velocity-dependent convective flux due to the moving coordinate system. Thus the equations of mass balance in regions P, E, T, S, R, and M are

$$\frac{\partial C^P}{\partial t} = \frac{1}{a}[J^{TP}(C^T,C^P) - J^{PT}(C^T,C^P)] - v\frac{\partial C^P}{\partial x} + D^P\frac{\partial^2 C^P}{\partial x^2}, \tag{9}$$

$$\frac{\partial C^E}{\partial t} = \frac{1}{a}[J^{SE}(C^S,C^E) - J^{ES}(C^S,C^E)] - v\frac{\partial C^E}{\partial x} + D^E\frac{\partial^2 C^E}{\partial x^2}, \tag{10}$$

$$\frac{\partial C^T}{\partial t} = \frac{1}{a}[J^{PT}(C^T,C^P) - J^{TP}(C^T,C^P) + J^{RT}(C^T,C^R) - J^{TR}(C^T,C^R)] - v\frac{\partial C^T}{\partial x} + D^T\frac{\partial^2 C^T}{\partial x^2}, \tag{11}$$

$$\frac{\partial C^S}{\partial t} = \frac{1}{a}[J^{ES}(C^S,C^E) - J^{SE}(C^S,C^E) + J^{MS}(C^S,C^M) - J^{SM}(C^S,C^M)] - v\frac{\partial C^S}{\partial x} + D^S\frac{\partial^2 C^S}{\partial x^2}, \tag{12}$$

$$\frac{\partial C^R}{\partial t} = \frac{1}{a}[J^{TR}(C^T,C^R) - J^{RT}(C^T,C^R)] - v\frac{\partial C^R}{\partial x} + D^R\frac{\partial^2 C^R}{\partial x^2} - C^R k^{R,evap} + \frac{fF}{aa_o^2}, \tag{13}$$

$$\frac{\partial C^M}{\partial t} = \frac{1}{a}[J^{SM}(C^S,C^M) - J^{MS}(C^S,C^M)] - v\frac{\partial C^M}{\partial x} + D^M\frac{\partial^2 C^M}{\partial x^2} - C^M k^{M,evap} + \frac{fF}{aa_o^2}, \tag{14}$$

where all C^α and $J^{\alpha\beta}$ depend explicitly on both lateral coordinate x and time t.

The above set of equations is solvable in principle with the appropriate set of boundary conditions. However, we further simplify the problem and gain physical insight by considering only two of the four mechanisms shown in Fig. 1. For our purposes it is sufficient to include one step-edge mechanism and one terrace-mediated mechanism to demonstrate the relative importance of each mechanism class. In the development here, we have chosen to include only the transitions (T↔P) and (S↔E); we neglect lateral step-edge transitions because we contend they are less important than vertical ones. This assumption eliminates the vertical diffusive fluxes in Eqs. (13) and (14) as well as the corresponding terms in the remaining equations.

Given this simplification, we make the following assertions:

(1) Lateral diffusion in layers other than the adatom layer provides a negligible contribution to segregation and we therefore set $D^\alpha=0$ for $\alpha=\mathrm{S,T,E,P}$. A rigorous treatment of diffusion in the current formalism is beyond the scope of this paper. One expects that diffusion can affect the actual shape of the concentration profile within a given layer; however it should not significantly affect the integrated amount of impurity in that region. The assertion breaks down in the case where there is a large diffusivity in, e.g., layer T and a small vertical exchange rate (T↔R) but rapid step-edge exchange rate, leading to a "short circuit" vertical pathway at the step edge. At high temperatures, such a short circuit mechanism could cause a disproportionate change in the integrated impurity concentration for that region. The result of this assertion is that the lateral diffusion terms can be removed from Eqs. (9)–(12).[44]

(2) The extent of the step-edge region approaches the dimension of a single unit cell in the plane, $w \to a_o$. This assertion basically says that the availability of step-edge-mediated mechanisms is limited to those atoms that are directly on the step edge. Thus we can treat regions S and E as discrete and convert the partial spatial derivative term in Eqs. (10) and (12) into a finite difference. In addition, the partial time derivative becomes a full derivative. The case of extended step-edge regions is treated in Appendix A.

(3) The total impurity content in adatom regions M and R does not significantly contribute to the overall surface excess or the segregation ratio. This allows us to ignore Eqs. (13) and (14) from the set of equations (9)–(14). Essentially the position-dependent adatom concentration in regions M and R for $x<L$ has no consequence other than to establish a steady-state concentration at $x=L$ through the balance of deposition, evaporation, and lateral diffusion. This value, plus the kinetics of lateral segregation at the moving step edge, determines how much impurity gets incorporated at the step edge, thus fixing the $x=0$ boundary of C^S. This in turn sets the scale for the concentration profiles in subsequent regions T, E, P, and bulk. The range of validity for this assertion is discussed in further detail in Appendix B.

From these assertions, Eqs. (9)–(14) are rewritten with their explicit variable dependencies as

$$\frac{\partial C^P(x,t)}{\partial t} = \frac{1}{a}[J^{TP}(C^T(x,t),C^P(x,t)) - J^{PT}(C^T(x,t),C^P(x,t))] - v\frac{\partial C^P(x,t)}{\partial x}, \tag{15}$$

$$\frac{dC^E(t)}{dt} = \frac{1}{a}[J^{SE}(C^S(t),C^E(t)) - J^{ES}(C^S(t),C^E(t))] - \frac{v}{a_o}\cdot[C^E(t) - C^T(L,t)], \tag{16}$$

$$\frac{\partial C^T(x,t)}{\partial t} = \frac{1}{a}[J^{PT}(C^T(x,t),C^P(x,t)) - J^{TP}(C^T(x,t),C^P(x,t))] - v\frac{\partial C^T(x,t)}{\partial x}, \tag{17}$$

$$\frac{dC^S(t)}{dt} = \frac{1}{a}[J^{ES}(C^S(t),C^E(t)) - J^{SE}(C^S(t),C^E(t))] - \frac{v}{a_o}\cdot[C^S(t) - C^{inc}], \tag{18}$$

where C^{inc} is the concentration of B atoms that is incident on the step edge at $x=L$. Equations (16) and (18) make the implicit assumption that there is continuity in concentration across the boundary at $x=L$.

The vertical diffusive fluxes, $J^{\alpha\beta}$, in the above equations are obtained from unimolecular rate theory.[21,45] Consider the (P→T) transition and assume the system lowers its energy by exchanging a B atom in region P with an A atom in region T, and likewise for E and S, respectively. The interchange flux from P to T is then given by

$$J^{PT}(C^T(x,t),C^P(x,t)) = C^P(z,t)\cdot[1 - a_o^2 a C^T(z,t)]\cdot \nu a \cdot \exp\left(-\frac{Q^{TP}}{k_B T}\right). \tag{19}$$

The reverse flux has the same form, but the barrier for this process includes the segregation energy, or the difference in redistribution potential between the two states $\Delta\mu'^{TP}$;[46]

$$J^{TP}(C^T(x,t),C^P(x,t)) = C^T(z,t)\cdot[1 - a_o^2 a C^P(z,t)]\cdot \nu a \cdot \exp\left(-\frac{(Q^{TP} + \Delta\mu'^{TP})}{k_B T}\right). \tag{20}$$

Similarly for the (S↔E) transition,

$$J^{ES}(C^S(t),C^E(t)) = C^E(t)\cdot[1 - a_o^2 a C^S(t)]\cdot \nu a \cdot \exp\left(-\frac{Q^{SE}}{k_B T}\right), \tag{21}$$

$$J^{SE}(C^S(t),C^E(t)) = C^S(t)\cdot[1 - a_o^2 a C^E(t)]\cdot \nu a \cdot \exp\left(-\frac{(Q^{SE} + \Delta\mu'^{SE})}{k_B T}\right). \tag{22}$$

In these cases, the assumption that a B atom has a lower energy in the T state forces $\Delta\mu'^{TP}$ to be a positive value.[47]

All concentrations are assumed dilute and the $(1 - a_o^2 a C^\alpha)$ terms in Eqs. (19) and (20) are set equal to unity, thereby making the diffusive fluxes linearly proportional to the concentrations.[48] In the steady state, the concentration of incident atoms equals the concentration entering the bulk, $C^{inc}=C_{bulk}$, and the dilute forms for Eqs. (19) and (20) are substituted into Eqs. (15)–(18), to yield a final set of equations to be solved:

$$0 = \frac{v_d^{TP}}{a_o}[k_e^{TP}\cdot C^T(x) - C^P(x)] - v\frac{d}{dx}C^P(x), \tag{23}$$

$$0 = \frac{-v_d^{TP}}{a_o}[k_e^{TP}\cdot C^T(x) - C^P(x)] - v\frac{d}{dx}C^T(x), \tag{24}$$

$$0 = C^S\cdot\frac{v_d^{SE}k_e^{SE}}{a_o} - C^E\cdot\left(\frac{v_d^{SE}}{a_o} + \frac{v}{a_o}\right) + \frac{v}{a_o}C^T(L), \tag{25}$$

$$0 = C^S\cdot\left(\frac{-v_d^{SE}k_e^{SE}}{a_o} - \frac{v}{a_o}\right) + C^E\cdot\left(\frac{v_d^{SE}}{a_o}\right) + \frac{v}{a_o}C_{bulk}, \tag{26}$$

where

$$k_e^{TP(\text{or}SE)} = \exp\left(\frac{-\Delta\mu'^{TP(\text{or}SE)}}{k_B T}\right), \tag{27}$$

$$v_d^{TP(\text{or}SE)} = \nu a_o \exp\left(\frac{-Q^{TP(\text{or}SE)}}{k_B T}\right) \tag{28}$$

are the equilibrium partition coefficient and the diffusive speed, respectively, as defined for the case of solidification.[46]

C. Concentration profiles

The problem has now been reduced to a set of coupled, linear ordinary differential equations for $C^P(x)$ and $C^T(x)$. We normalize these equations by the constant C_{bulk} and the solution becomes

$$\frac{C^P(x)}{C_{bulk}} = -\mathbb{A}e^{-\kappa x} + k_e^{TP}\mathbb{B}, \tag{29}$$

$$\frac{C^T(x)}{C_{bulk}} = \mathbb{A}e^{-\kappa x} + \mathbb{B}, \tag{30}$$

where we have substituted the in-plane decay length

$$\kappa = \frac{v_d^{TP}}{v a_o}(1 + k_e^{TP}). \tag{31}$$

The constants, $\mathbb{A}$ and $\mathbb{B}$, are determined from the boundary conditions $C^T(a_o)=C^S$ and $C^P(a_o)=C^E$, or

$$\frac{C^S}{C_{bulk}} = \mathbb{A}e^{-\kappa a_o} + \mathbb{B}, \tag{32}$$

$$\frac{C^E}{C_{bulk}} = -\mathbb{A}e^{-\kappa a_o} + k_e^{TP}\mathbb{B}. \tag{33}$$

Finally, the solution of the simultaneous set of equations given by (25), (26), (32), and (33) provides expressions in closed form for $\mathbb{A}$ and $\mathbb{B}$:

$$\mathbb{A} = e^{\kappa a_o}\frac{k_e^{TP}\left(\frac{v}{v_d^{SE}} + 1\right) - k_e^{SE} - \frac{v}{v_d^{SE}}}{e^{-\kappa(L-a_o)}\left(\frac{v}{v_d^{SE}} + k_e^{SE} - k_e^{TP}\right) + k_e^{TP}\left(1 + k_e^{SE} + \frac{v}{v_d^{SE}}\right)}; \tag{34}$$

$$\mathbb{B} = \frac{\frac{v}{v_d^{SE}}(1 + e^{-\kappa(L-a_o)}) + 1 + k_e^{SE}}{e^{-\kappa(L-a_o)}\left(\frac{v}{v_d^{SE}} + k_e^{SE} - k_e^{TP}\right) + k_e^{TP}\left(1 + k_e^{SE} + \frac{v}{v_d^{SE}}\right)}. \tag{35}$$

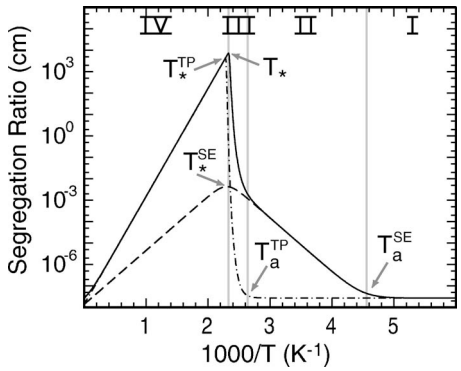

FIG. 2. Possible temperature-dependent behavior for the segregation ratio. The solid line represents the predictions of this model assuming energies of $\Delta\mu'^{TP}$, $Q^{TP}=1$ eV and $\Delta\mu'^{SE}$, $Q^{SE}=0.5$ eV, a deposition rate of 1 monolayer/second and a terrace length of $25a_o$. The dashed line shows the plot of Eq. (49) representing the model with the single (S↔E) transition. The dot-dashed line shows Eq. (44) representing the model with the single (T↔P) transition. The roman numerals label the segregation regimes described in the text and summarized in Table I.

D. Surface excess and segregation ratio

It remains to determine the Gibbsian surface excess, Γ, from Eq. (2). In this formulation of the model, which ignores the adatom regions M and R, everywhere there are two layers for the nonbulk region; hence $\zeta=2a$. From Eq. (2),

$$\frac{\Gamma}{C_{bulk}}=\frac{1}{L}\left(\int_{-a}^{0}\int_{0}^{a_o}\frac{C^S}{C_{bulk}}dxdz+\int_{-a}^{0}\int_{a_o}^{L}\frac{C^T(x)}{C_{bulk}}dxdz+\int_{-2a}^{-a}\int_{0}^{a_o}\frac{C^E}{C_{bulk}}dxdz+\int_{-2a}^{-a}\int_{a_o}^{L}\frac{C^P(x)}{C_{bulk}}dxdz\right)-2a. \tag{36}$$

This equation is integrated to obtain

$$\frac{\Gamma}{C_{bulk}}=\frac{1}{L}\left(a_o a\frac{C^S}{C_{bulk}}+a\int_{a_o}^{L}\frac{C^T(x)}{C_{bulk}}dx+a_o a\frac{C^E}{C_{bulk}}+a\int_{a_o}^{L}\frac{C^P(x)}{C_{bulk}}dx\right)-2a. \tag{37}$$

After substituting Eqs. (29), (30), (32), and (33) and solving the integrals, the Gibbsian excess reduces to

$$\frac{\Gamma}{C_{bulk}}=a\mathbb{B}(1+k_e^{TP})-2a. \tag{38}$$

Finally the segregation ratio is obtained from Eq. (8):

$$r=a(1+k_e^{TP})\mathbb{B}. \tag{39}$$

Equations (38) and (39) represent the major result of this model.

One of the main consequences of the model is a transition between kinetically limited and equilibrium segregation. When temperature is varied at constant flux and step spacing, multiple transition temperatures correspond to the kinetic transition for each individual segregation mechanism. The segregation ratio exhibits not only temperature-dependent behavior, but also velocity and miscut dependence as observed experimentally.[49,50] In the next section this behavior is explored in further detail.

IV. GENERAL LIMITING BEHAVIOR AND SEGREGATION REGIMES

Figure 2 shows some general temperature-dependent behavior of the segregation ratio as predicted by this model for arbitrary input energy barriers. A transition occurs at a temperature T_* that separates the kinetically limited segregation regime at lower temperatures and the equilibrium segregation regime at higher temperatures (regimes III and IV). With the appropriate choice of energies, it is possible to introduce a second transition temperature within the kinetically limited regime, at which the predominant segregation mechanism undergoes a change from terrace-mediated (T↔P) (regime III) to step-edge-mediated (S↔E) (regime II). In order to gain insight into the results of this model, it is useful to look at a few physical limits. These limits include T→∞ and T→0, as well as considering large differences in the energy barriers for the two mechanisms (e.g., $Q^{SE}\to\infty$ or $Q^{TP}\to\infty$).

A. Limit 1: T→∞

In the limit that T→∞, the atoms rapidly surmount any barrier to motion and the energy differences among configurations become negligible; hence the system does not maintain any concentration gradients. In this limit the surface excess vanishes as all the impurity atoms are evenly distributed throughout the growing film. Mathematically, from Eqs. (27) and (28), in this limit k_e^{SE} and $k_e^{TP}\to 1$, and v_d^{SE} and $v_d^{TP}\to \nu a_o$. Then substituting into Eq. (35), we find $\mathbb{B}\to 1$. Then by Eqs. (38) and (39), $\Gamma\to 0$ and $r\to 2a$.

B. Limit 2: T→0

In this limit, the temperature of the system is so low that impurity atoms have no mobility during growth and all impurity gets trapped in the growing film. Under these conditions, we would expect that there is no segregation and, correspondingly, no surface excess. Here, k_e^{SE}, k_e^{TP}, v_d^{SE}, $v_d^{TP}\to 0$ and, by Eq. (31), $\kappa\to 0$ as well. Then by Eq. (35), $\mathbb{B}\to 2$, and $\Gamma\to 0$ and $r\to 2a$ as expected.

C. Limit 3: $Q^{SE}\to\infty$

In this limit we probe the behavior of the mid-terrace (T↔P) mechanism alone by turning off the (S↔E) transition. The activation barrier for (S↔E) is allowed to diverge so that $v_d^{SE}\to 0$ and $v/v_d^{SE}\to\infty$. For finite temperatures, k_e^{SE} and $k_e^{TP}\ll 1$ and Eq. (35) becomes

$$\mathbb{B}\to\frac{1+e^{-\kappa(L-a_o)}}{e^{-\kappa(L-a_o)}+k_e^{TP}}. \tag{40}$$

This equation is combined with Eq. (39) to yield

$$r \to a\frac{1+e^{-\kappa(L-a_o)}}{e^{-\kappa(L-a_o)}+k_e^{TP}}. \tag{41}$$

This result is plotted as the dot-dashed line in Fig. 2. For this single mechanism, there exists a transition between a kinetically limited regime and an equilibrium regime. Two turning points are observed on this plot. The first, T_a^{TP}, is the temperature above which this mechanism is activated and segregation begins. The second location, T_*^{TP}, is the transition temperature above which equilibrium segregation occurs.

Through Eq. (41), we find that as $e^{-\kappa(L-a_o)}$ approaches 1; we return to limit 2. Therefore, the temperature at which this mechanism becomes activated is given by $\kappa=1/(L-a_o)$. We recognize that for a terrace of length L, the step velocity is given by

$$v = RL, \tag{42}$$

where R is the net deposition rate (monolayers/second) of all species. Then in the limit that $L \gg a_o$ we find

$$\frac{1}{T_a^{TP}} = \frac{k_B \ln\left(\frac{\nu}{R}\right)}{Q^{TP}}. \tag{43}$$

For temperatures above T_a^{TP}, $e^{-\kappa(L-a_o)} \ll 1$, and the segregation ratio becomes

$$r \to \frac{a}{e^{-\kappa(L-a_o)}+k_e^{TP}}. \tag{44}$$

The transition temperature between kinetically limited and equilibrium segregation is governed by the relationship between $e^{-\kappa(L-a_o)}$ and k_e^{TP}. In this limit,

$$r_{\text{eq}} \to \frac{a}{k_e^{TP}} \quad \text{for } T > T_*^{TP}, \tag{45}$$

$$r_{\text{kin}} \to a e^{\kappa(L-a_o)} \quad \text{for } T < T_*^{TP}, \tag{46}$$

where r_{eq} is the segregation length in the equilibrium segregation regime and r_{kin} is the segregation length in the kinetically limited regime. The transition temperature is determined by equating Eqs. (45) and (46). Applying the definitions of κ and k_e^{TP} we find the transcendental equation,

$$\frac{RL\Delta\mu'^{TP}}{\nu(L-a_o)} = k_B T_*^{TP} \exp\left(\frac{-Q^{TP}}{k_B T_*^{TP}}\right). \tag{47}$$

It should be noted that the predicted behavior for the single ($T \leftrightarrow P$) transition given by Eq. (44) is identical to Eq. (7) in Jorke's treatment[28] with the additional condition that the Jorke model does not include a step-edge region (i.e., $a_o \to 0$).

D. Limit 4: $Q^{TP} \to \infty$

In this limit, we turn off the mid-terrace ($T \leftrightarrow P$) transition and enable the step edge mediated ($S \leftrightarrow E$) transition. Here we have the similar condition as before that k_e^{TP} and $k_e^{SE} \ll 1$, yet because $v_d^{TP} \to 0$, $e^{-\kappa(L-a_o)} \to 1$. In this limit

$$\mathbb{B} \to \frac{2\frac{v}{v_d^{SE}}+1}{(1+k_e^{TP})\left(\frac{v}{v_d^{SE}}+k_e^{SE}\right)}. \tag{48}$$

When we combine this equation with Eq. (39), we find the segregation ratio

$$r \to a\frac{2\frac{v}{v_d^{SE}}+1}{\frac{v}{v_d^{SE}}+k_e^{SE}}. \tag{49}$$

The result of Eq. (49) is nearly identical to the equation (7.46) in Tsao's model[30] with the additional factor of 2 related to the fact that $\zeta=2a$ in our case. This equation is plotted in Fig. 2 as a dashed line, and again our model predicts a transition between kinetically limited behavior and equilibrium behavior for this single mechanism. For $v/v_d^{SE} \gg 1$, we return to limit 2 where the mechanism has been turned off and there is no segregation. Thus the mechanism becomes activated as $v/v_d^{SE} \to 1$. We use this relation to determine that the temperature to activate this mechanism is given by

$$\frac{1}{T_a^{SE}} = \frac{k_B \ln\left(\frac{\nu a}{RL}\right)}{Q^{SE}}. \tag{50}$$

In the temperature regime near the transition, T_*^{SE}, both k_e^{SE} and v/v_d^{SE} are $\ll 1$. Therefore, the numerator of Eq. (49) approaches unity while the relative magnitudes of two terms in the denominator determine whether segregation is in a kinetically limited or equilibrium regime. Thus,

$$r_{\text{eq}} \to \frac{a}{k_e^{SE}} \quad \text{for } T > T_*^{SE}, \tag{51}$$

$$r_{\text{kin}} \to \frac{a v_d^{SE}}{v} \quad \text{for } T < T_*^{SE}, \tag{52}$$

and the transition temperature is given by equating these two expressions to find

$$T_*^{SE} = \frac{\Delta\mu'^{SE}+Q^{SE}}{k_B \ln\left(\frac{a\nu}{v}\right)}. \tag{53}$$

E. Temperature dependence of segregation behavior

The sample plot of the segregation ratio using arbitrary energies (Fig. 2) for the full two-mechanism model shows four regimes denoted I–IV. If we consider the results of the previous limiting cases, the segregation behavior at these different temperatures can be understood. At the lowest temperatures, there is not enough thermal energy to overcome the activation barriers for exchange and therefore no segre-

TABLE I. Approximate equations governing segregation behavior in different temperature regimes. The transition conditions denote the relevant mathematical equation that distinguishes one regime from the previous one. The physical interpretation tells us which mechanism is active and whether it is kinetically limited (kin) or in its equilibrium segregation (eq) regime.

Regime	Segregation ratio	Transition condition	Physical interpretation
I	$2a$		(S↔E) off, (T↔P) off
II	av_d^{SE}/v	$v/v_d^{SE}=1$	(S↔E) kin, (T→P) off
IIb	a/k_e^{SE}	$v/v_d^{SE}=k_e^{SE}$	(S↔E) eq, (T↔P) off
III	$a/\{e^{-\kappa(L-a_o)}[(v/v_d^{SE})+k_e^{SE}]\}$	$\kappa(L-a_o)=1$	(S↔E) kin or eq, (T↔P) kin
IIIb	$a/k_e^{TP}(1-e^{-\kappa(L-a_o)})$	$[(v/v_d^{SE})+k_e^{SE}]/k_e^{TP}=(1-e^{-\kappa(L-a_o)})$	(S↔E) kin or eq, (T↔P) kin
IV	a/k_e^{TP}	$k_e^{TP}/[(v/v_d^{SE})+k_e^{SE}]=e^{-\kappa(L-a_o)}$	(S↔E) kin or eq, (S↔E) eq

gation occurs. In this regime, $r\rightarrow 2a$. Once the temperature increases beyond T_a^{SE}, a transition to regime II occurs as the step-edge-mediated mechanism becomes active in its kinetically limited regime. At somewhat higher temperatures (regime III), the terrace mechanism at T_a^{TP} activates. This mechanism dominates the overall segregation behavior provided the terrace length is larger than the lattice spacing. Ultimately, we reach the transition to the equilibrium segregation regime at T_* and move into regime IV. In this regime, the segregation behavior is dominated by the equilibrium segregation regime of the (T↔P) transition. The reason that the step edge region does not play an important role in the segregation behavior in the equilibrium regime is that the terrace region is the last place an atom can make an exchange before becoming trapped in the bulk. Therefore, regardless of what segregation behavior occurs at the step edge, atoms subsequently have the entire terrace length to reequilibrate with region T. A summary of these regimes and the governing equations are given in Table I.

It remains to find the overall transition temperature, or temperature of maximum segregation, T_*, in a similar fashion as before. Near T_*, k_e^{SE}, $k_e^{TP}\ll 1$, but also, from limits 3 and 4, $e^{-\kappa(L-a_o)}$ and v/v_d^{SE} are also $\ll 1$. Therefore, the segregation ratio is rewritten in this regime as

$$r=\frac{a}{e^{-\kappa(L-a_o)}\left(\frac{v}{v_d^{SE}}+k_e^{SE}\right)+k_e^{TP}}. \tag{54}$$

This equation is similar to the equation for the (T↔P) transition [limit 3, Eq. (44)] with a slight modification to the $e^{-\kappa(L-a_o)}$ term. This modification accounts for the fact that the step edge region is providing additional atomic reorganization for the overall system. Again, the regime in which we find ourselves depends on the relative magnitudes of the two terms in the denominator. As before, we calculate the transition temperature by finding the temperature, T_*, that satisfies the equation

$$\frac{k_e^{TP}}{\left(\frac{v}{v_d^{SE}}+k_e^{SE}\right)}=e^{-\kappa(L-a_o)}, \tag{55}$$

where the denominator on the left side of the equation will be dominated by either the v/v_d^{SE} or k_e^{SE} term depending on whether the step-edge mechanism is in the kinetically limited or equilibrium segregation regime.

The presence of four distinct regimes in the temperature dependence of the segregation ratio depends on the relative energies used in the calculation. The physical interpretation of the energy hierarchy is written in terms of the transition temperatures and equilibrium segregation coefficients, namely, $T_a^{SE}<T_a^{TP}$, $T_*^{SE}>T_a^{TP}$, and $k_e^{TP}<k_e^{SE}$. If the energies are such that one or more of these conditions is no longer valid, we either get additional regimes in the temperature dependence or fewer regimes. Figure 3 shows representative plots for the temperature dependence of the segregation ratio if one assumes alternate relative energies for the system. The energies have been chosen to catalogue the possible behavior exhibited by the model and are listed in Table II.

In Fig. 3(a), one observes the situation when one mechanism dominates the other mechanism. In this case, as the temperature is raised, the terrace-mediated mechanism becomes activated well before the step-edge mechanism and clearly dominates the resulting behavior. Although lower atomic coordination at step edges might imply that the step-edge mechanism should always exhibit a lower activation energy than the terrace mechanism, unusual circumstances, e.g., strain effects on the activation barriers, could cause such a scenario. In addition, the dependence of segregation behavior on terrace length can cause similar effects as will be discussed later.

In Figs. 3(b)–3(e), the system is shown for cases in which, as the temperature is raised, the step-edge mechanism becomes activated before the terrace-mediated processes. This condition is the same as for Fig. 2; however, by modifying the relative magnitude of the energies, alternative regimes

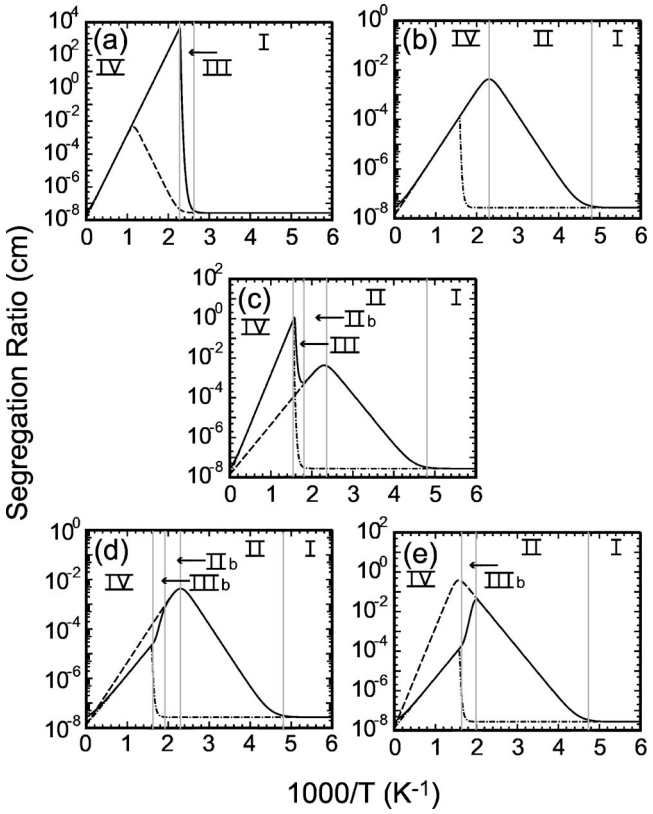

FIG. 3. Alternate possibilities for temperature-dependent segregation behavior. Dot-dashed lines represent the model with single (T↔P) transition, dashed line represents the model with single (S↔E) transition. Roman numerals denote the segregation regimes listed in Table I. Deposition rate of 1 monolayer/second, terrace length of $25a_o$, and energies given in Table II.

are displayed. In Figs. 3(b) and 3(c), the terrace process becomes activated and reaches the equilibrium segregation regime of the step-edge mechanism (regime IIb). Depending on the magnitude of k_e^{TP} relative to the magnitude of k_e^{SE}, the segregation ratio will exhibit different behavior. Figure 3(b) shows the special case when the two values are equal. In this case, there is no additional segregation regime and the equilibrium regime IV remains for increasing temperatures. In Fig. 3(c), $k_e^{TP} < k_e^{SE}$, and when the terrace-mediated mechanism becomes activated, it pushes the system back into a kinetically limited regime as shown by the reemergence of regime III. Once the temperature reaches T_*^{TP}, the system returns to the equilibrium regime for the terrace process and returns to regime IV.

In Figs. 3(d) and 3(e), $k_e^{TP} > k_e^{SE}$ and a new regime appears in the segregation ratio temperature behavior. The onset of the terrace mediated mechanism for these sample energies leads to a kinetically limited segregation regime in which the segregation ratio decreases with respect to increasing temperature as denoted by regime IIIb. This occurs whether the step mediate process is in an equilibrium segregation regime [Fig. 3(d)] or a kinetically limited segregation regime [Fig. 3(e)]. Such behavior is opposite that which is expected for kinetically limited segregation regimes due to an inversion in the chemical potential difference between T and P. This occurs due to the large concentration of B atoms that convectively flow from S into T. Recall the chemical potential difference between T and P is given by

$$\Delta\mu^{TP} = \Delta\mu'^{TP} - k_B T \ln \frac{C^T}{C^P}. \tag{56}$$

When the concentration in T is sufficiently large, the sign of $\Delta\mu^{TP}$ will change indicating a change in the direction of the net driving force on B atoms from T into P. We refer to this regime as the "chemical potential inversion" regime. Thus, when the temperature is high enough to allow the terrace mediated mechanism to exchange atoms, the net flux from T into P causes the segregation ratio to decrease as temperature is increased.

The possibility of a chemical potential inversion regime indicates that a single measurement of the sign of the slope in r vs (T) is insufficient to conclusively determine whether one is in a kinetically limited or equilibrium segregation regime. A more complete data set (e.g., see rate dependence below) or additional information about the relative energies would be needed to unambiguously make a determination. The explicit form for the segregation ratio in this regime is given in Table I with the appropriate transition conditions given in Table III.

TABLE II. Energies used for Q^{TP}, $\Delta\mu'^{TP}$, Q^{SE}, and $\Delta\mu'^{SE}$ in generating Figs. 2 and 3 along with the temperature-dependent segregation ratio regimes that are present in the plot.

Figure	Q^{TP} (eV)	$\Delta\mu'^{TP}$ (eV)	Q^{SE} (eV)	$\Delta\mu'^{SE}$ (eV)	Regimes
2	1.0	1.0	0.5	0.5	I, II, III, IV
3(a)	1.0	1.0	1.0	1.0	I, III, IV
3(b)	1.5	0.5	0.5	0.5	I, II, IV
3(c)	1.5	1.0	0.5	0.5	I, II, IIb, III, IV
3(d)	1.5	0.4	0.5	0.5	I, II, IIb, IIIc, IV
3(e)	1.5	0.5	0.5	1.0	I, II, IIIb, IV

F. Deposition rate dependence

Figure 4 shows a sample plot of the deposition rate dependence at a fixed temperature for the same parameters given in Fig. 2. The labelled regimes on the plot directly correspond to the previously discussed segregation regimes. The connection is readily apparent in Fig. 5 for which the temperature dependence is plotted for a variety of growth rates. One observes that changes in the deposition rate cause a shift in the transition and activation temperatures. Thus the segregation regime associated with a fixed temperature (solid vertical line in Fig. 5) changes due to the effects of growth rate. The rate at which the transitions occur are given in Table III with the relevant equation numbers.

At the highest deposition rates $(R \to \infty)$, regime I, there is insufficient time for the atoms to segregate before becoming buried by the moving step edge [see Eq. (42)]. This case is equivalent to the limit $T \to 0$ and thus the segregation ratio $r \to 2a$ and it is independent of the deposition rate. As the

TABLE III. Equations governing the temperature and deposition rate transition between segregation regimes. For regime IV, the transition temperature and deposition rate are solutions to the transcendental functions in the given condition. The given equation numbers refer to the relevant equations in the text. In all cases, we have assumed $L \gg a_o$. In regimes IIIb and IV, T_* and r^* are obtained by solving the given equation.

Regime	Transition temperature	Transition deposition rate	Equations
I	$T \to 0$	$R \to \infty$	
II	$T_a^{SE} = Q^{SE}/[k_B \ln(\nu a/RL)]$	$R_a^{SE} = (\nu a_o/L) \exp(-Q^{SE}/k_B T)$	(50) and (57)
IIb	$T_*^{SE} = (\Delta\mu'^{SE} + Q^{SE})/[k_B \ln(a\nu/RL)]$	$R_*^{SE} = (\nu a_o/L) \exp[-(\Delta\mu'^{SE} + Q^{SE})/k_B T]$	(53)
III	$T_a^{TP} = Q^{TP}/[k_B \ln(\nu/R)]$	$R_a^{TP} = \nu \exp(-Q^{SE}/k_B T)$	(43)
IIIb	$[(v/v_d^{SE}) + k_e^{SE}]/k_e^{TP} = (1 - e^{-\kappa(L-a_o)})$	$[(v/v_d^{SE}) + k_e^{SE}]/k_e^{TP} = (1 - e^{-\kappa(L-a_o)})$	
IV	$k_e^{TP}/[(v/v_d^{SE}) + k_e^{SE}] = e^{-\kappa(L-a_o)}$	$k_e^{TP}/[(v/v_d^{SE}) + k_e^{SE}] = e^{-\kappa(L-a_o)}$	(55)

deposition rate decreases, eventually we reach a transition to regime II in which the $(S \leftrightarrow E)$ transition occurs fast enough for impurity atoms to evade the moving step edge, but the $(T \leftrightarrow P)$ transition is frozen by the motion of the step edge. This case is equivalent to temperature regime II in which the $(S \leftrightarrow E)$ transition is activated, but the $(T \leftrightarrow P)$ transition does not have enough thermal energy to overcome the barrier. The segregation ratio in this regime is given in Eq. (52) showing a rate dependence of $r \propto R^{-1}$.

As the deposition rate is further reduced, we enter regime III, in which the terrace mediated transitions occur fast enough for impurity atoms to evade the slowly moving growth front. In this case, the segregation ratio is given in Table I with a steeper rate dependence. Finally, at the slowest growth rates, the system has enough time to reach the equilibrium segregation regime and we return to the growth-rate-independent regime IV with $r \to 2a$. A full summary of the segregation ratio behavior as a function of growth rate is given in Table I.

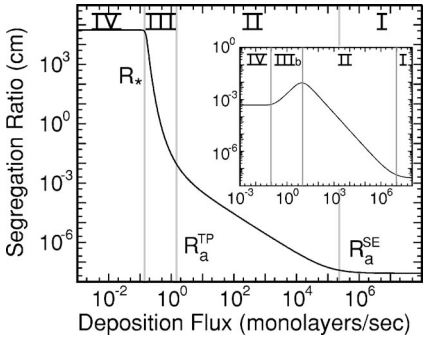

FIG. 4. General deposition rate behavior for the segregation ratio. The solid line represents the predictions of this model assuming energies of $\Delta\mu'^{TP}$, $Q^{TP} = 1$ eV, and $\Delta\mu'^{SE}$, $Q^{SE} = 0.5$ eV, a temperature of 400 K, and a terrace length of $25a_o$. The Roman numerals label the segregation regimes described in the text and summarized in Table I. The inset depicts model predictions for the energies given in Fig. 3(e) at a temperature of 555 K showing the inverse deposition rate dependence of regime IIIb.

The transition deposition rates between the regimes can be determined in a similar fashion as those for the temperature dependence. The transition between regimes I and II occurs at the onset of the $(S \leftrightarrow E)$ transition, R_a^{SE}. As in Eq. (50), the condition for transition between these regimes is given by $v/v_d^{SE} \to 1$. The equation can be solved for R_a^{SE} at fixed temperature,

$$R_a^{SE} = \frac{\nu a_o}{L} \exp\left(-\frac{Q^{SE}}{k_B T}\right). \tag{57}$$

The conditions for the transitions between II-III and III-IV given in Eqs. (43) and (55) can similarly be solved for R_a^{TP} and r^* and are given in Table III.

Additional flux dependence regimes corresponding to the additional temperature regimes discussed in the previous section are possible depending on the barrier height (see Tables I and III). In regime IIb, the segregation is in the equilibrium regime and therefore independent of the growth rate.

Interestingly, regime IIIb exhibits a growth rate dependence in which the segregation ratio decreases as the growth decreases (inset of Fig. 4). Again, this behavior is a result of the chemical potential inversion which causes a driving force

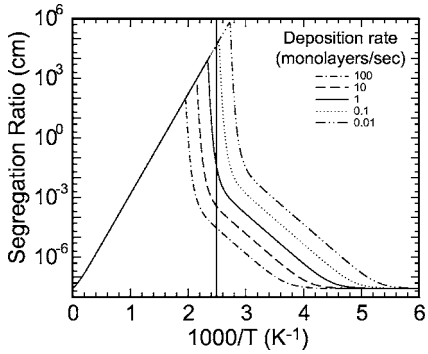

FIG. 5. Temperature dependence of segregation ratio for different growth rates. The energies are the same as in Fig. 4. The solid line indicates the temperature at which the data for Fig. 4 are taken.

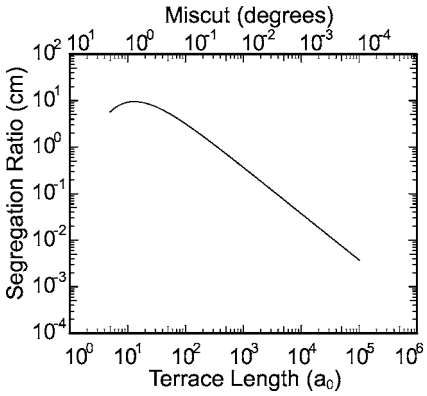

FIG. 6. Segregation ratio as a function of the terrace length for energies given in Fig. 4 at $1000/T=2.4$.

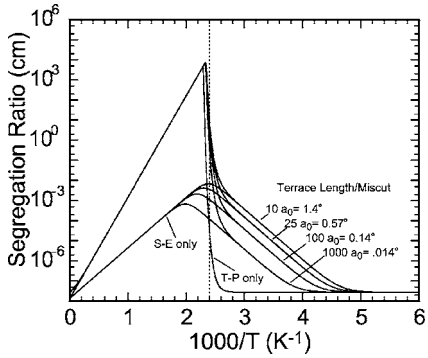

FIG. 7. Temperature dependence of the segregation ratio for terrace lengths. The energies are the same as in Fig. 4. The vertical dashed line represents the temperature plotted in Fig. 6. Subplot of terrace only $[(T\leftrightarrow P)]$ and step-edge only $[(S\leftrightarrow E)]$ segregation show effects on individual mechanisms.

for atoms to bury themselves in region P rather than segregate to region T. Thus, as the rate decreases, atoms have more time to exchange and move toward region P instead of segregating toward T.

G. Terrace length dependence

The general behavior of the segregation ratio as a function of terrace length can be obtained from the expressions for r given in Table I. The terrace length enters r implicitly through the step velocity in Eq. (42). One readily observes that the segregation ratio is independent of the terrace length in regimes I, IIb, and IV. In regime II, the segregation ratio is inversely proportional to the step velocity and therefore inversely proportional to the terrace length at constant R. This behavior is expected because only the step-edge-mediated mechanism is active. Thus an increase in L effectively decreases the number of active sites on the surface, thereby decreasing the overall amount of segregation.

Regime III shows a more complicated dependence on L (Fig. 6). In this case, we see that at the largest terrace lengths, the segregation ratio varies inversely with L. As the terrace length decreases, the segregation ratio levels off and in fact begins to decrease. The exhibited behavior in regime III can be understood by realizing that a change in the terrace length will greatly affect the step-edge contribution to the segregation behavior while having a much smaller effect on the terrace-mediated processes. This effect is shown graphically in Fig. 7 for different terrace lengths. The purely $(T\leftrightarrow P)$ segregation does not change significantly with L, whereas the $(S\leftrightarrow E)$ segregation shifts to higher temperatures as L increases. The result of this is that the temperature range spanned by regime III does not change significantly with terrace length as it does for the growth rate dependence (Fig. 4).

Equations (46) and (52) give the segregation ratio for the individual $(T\leftrightarrow P)$ and $(S\leftrightarrow E)$ transitions in their kinetically limited regimes. Because κ is proportional to $1/L$, the product $\kappa(L-a_0)$ is independent of L to first order for large L. Thus, the $(T\leftrightarrow P)$ transition is only slightly affected by changes in the terrace length in the kinetically limited regime. In contrast, the $(S\leftrightarrow E)$ transition clearly shows $1/L$ dependence in the kinetically limited regime. Then in regime III where both mechanisms are active, the product of their behavior will follow similar behavior to the $(S\leftrightarrow E)$ transition for large L. Depending on T_*^{SE} the segregation ratio will either be independent of L or inversely dependent on L.

To deal with the case of L small (i.e., high miscut), one needs to further analyze the expression for r in regime III. Equation (54) can be rewritten with explicit L dependence,

$$r = a\exp\left(\frac{v_d^{TP}}{a_0 R}\right)\exp\left(-\frac{v_d^{TP}}{RL}\right)\left(\frac{RL}{v_d^{SE}}+k_e^{SE}\right)^{-1}. \qquad (58)$$

For small L, the second exponential factor on the rhs no longer approaches unity and we observe a decaying exponential behavior with respect to L that dominates the behavior. Therefore, the segregation ratio will decrease as L decreases in this regime.

V. COMPARISON TO EXPERIMENT

A. Temperature dependence

Data for the segregation ratio of Sb in Si(001) and P in Si(001) have been obtained from the literature[32,51–53] and are shown in Figs. 8 and 9. The data for Sb demonstrate the rich behavior that is possible in real systems, showing multiple slopes in the kinetically limited regime. The solid line in the plot shows a good fit of our model to the experimental data using parameters given in Table IV. Therefore, applying our previous analysis to the model, we may interpret the apparent anomalous low temperature behavior as the presence of a step-edge-mediated mechanism that works in parallel with a terrace mechanism but has a lower activation barrier. This is consistent with the picture of a step edge on a surface where an edge atom has to break fewer bonds in comparison to a terrace atom in order to make an exchange.[35]

Furthermore, our fit demonstrates that $\Delta\mu'^{TP} > \Delta\mu'^{SE}$. This indicates that the Sb atoms feel less of a driving force between two states at a step edge in comparison to atoms in the mid-terrace, which is again consistent with the bonding structure at a step edge. Based on the available data, we consider $\Delta\mu'^{TP}$ to be a lower limit because we do not have

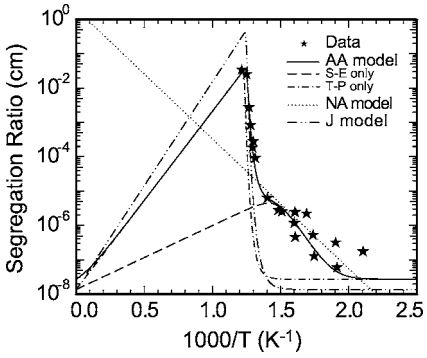

FIG. 8. Fit of temperature-dependent segregation ratio for Sb in Si(001). The symbols represent experimental data obtained from Refs. 51–53. Fitting parameters for J model (Ref. 28) are E_A =1.78 eV, E_I=1.2 eV, and $\nu=2\times10^{12}$ s^{-1}. Fitting parameters for NA model (Ref. 32), are E_{seg}=0.75 eV, Δ_o=2 cm, and ν=1.6 $\times10^{14}$ s^{-1}. Fitting parameters for the current model are given in Table IV. Dashed lines labeled S-E and T-P represent single (S↔E) and (T↔P) transitions.

sufficient data in the equilibrium segregation regime. An increase in $\Delta\mu'^{TP}$ would have the effect of increasing the slope in regime IV (see Table I) and a shift in the transition temperature toward higher temperatures, neither of which can be determined from the data.[54]

The fits obtained through this unified model show significant improvement over earlier attempts that employ single segregation mechanisms.[28,32] The dot-dashed line shows a best fit to the data using the Jorke model (terrace only). In this case, the model can sufficiently fit the higher temperature regimes, but insufficiently describes the data at lower temperatures. In the case of the surface-mediated model of Nutzel and Abstreiter (dotted line), the model is able to fit only the low-temperature regime, but is unable to handle the greater segregation at higher temperatures.

In order to generate the fits of our model to the experimental data, we have used only four free fitting parameters corresponding to Q^{TP}, $\Delta\mu'^{TP}$, Q^{SE}, and $\Delta\mu'^{SE}$, whereas previous unsuccessful model fits use three[28] and two[32] fitting parameters. The values we obtain, 1.9, 1.03, 1.19, and 0.37 eV, respectively, are consistent with previously reported barrier measurements and calculations for the different segregation mechanisms. Because the unified model is not based on a detailed kinetic pathway, these energy barriers should be considered a weighted average over all possible kinetic pathways that enable the exchange of atoms between (S↔E) or (T↔P). First principles calculations are possible to determine the energies independently, thereby permitting an independent method of obtaining and interpreting these energy values.

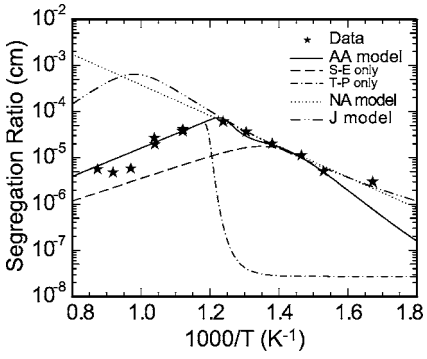

FIG. 9. Fit of temperature-dependent segregation ratio for P in Si(001). The symbols represent experimental data obtained from Ref. 32. Fitting parameters for J model (Ref. 28) are E_A=0.1 eV, E_I=1.0 eV, and ν=26.5 s^{-1}. Fitting parameters for NA model (Ref. 32) are E_{seg}=0.66 eV, Δ_o=0.8 cm, and $\nu=1.6\times10^{14}$ s^{-1}. Fitting parameters for the current model are given in Table IV. Dashed lines labeled S-E only and T-P only represent the single (S↔E) and (T↔P) transitions.

TABLE IV. Parameters used for generating data fits from model

Fitting parameters				
	Q^{TP} (eV)	$\Delta\mu'^{TP}$ (eV)	Q^{SE} (eV)	$\Delta\mu'^{SE}$ (eV)
Sb in Si(001)	1.9	1.03	1.19	0.37
P in Si(001)	2.0	0.61	1.17	0.48

Fixed parameters				
a_o (cm)	a (cm)	L	R $\left(\frac{\text{monolayer}}{\text{second}}\right)$	ν (s^{-1})
5.432×10^{-8}	1.358×10^{-8}	$25a_o$	1	1×10^{13}

It is necessary to make an explicit assumption about the surface structure in order to input a value for the terrace length. In all cases we have assumed a fixed terrace length as a function of time, temperature, and flux. Clearly this may not be the case, particularly at low temperatures and high fluxes where layer-by-layer growth is possible. In order to accommodate a nonconstant terrace length, we can introduce an explicit temperature and flux dependence to the terrace length in the model [for example, $L\propto(D/F)^n$ (Refs. 55 and 56)]. Such a process would introduce another arbitrary fitting parameter as additional information from experiments would be required to determine the relevant constant. Alternatively, experiments with detailed STM studies can be used to directly measure the terrace length.[57]

The fitting behavior for phosphorous shows similar results. Previous models are unable to fit the data across the available temperature regimes. For instance, the terrace-mediated model is able to fit the low-temperature regime, but requires the input of nonphysical energies (0.1 eV) and attempt frequencies (26.5). Similarly, the NA model is able to fit the low-temperature data, but does not predict a transition to equilibrium segregation and is unable to describe the high-temperature regimes. Based on the fit from our unified model, the onset of the terrace-mediated mechanism is much more slight in comparison to the Sb case and rapidly proceeds into the equilibrium regime. It is interesting to note that the activation barrier energies Q^{TP} and Q^{SE} are almost the same as those in the Sb case whereas $\Delta\mu'^{TP}$ and $\Delta\mu'^{SE}$ are quite different (Table IV).

It appears that for Si(001), the barrier heights do not vary markedly among the segregating species. This may indicate

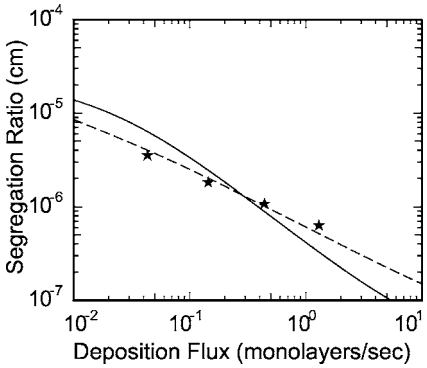

FIG. 10. Fit of deposition-flux-dependent segregation ratio for Sb in Si(001). The symbols represent experimental data obtained from Ref. 32. Parameters were fixed to those of Table IV. Best fit values were obtained for $1000/T=1.69$. Dashed line represents fit using the same parameters but allowing the terrace length to vary as the deposition rate, $L \propto R^{-1/3}$.

the dominance of a particular kinetic pathway that is the same for both segregating species. In contrast, the P has a very different energy well depth near the surface compared to Sb, which should be expected due to differences in both chemistry and size.

B. Flux dependence

The flux dependence at constant T has been measured for Sb and P in Si(001) (Ref. 32) and plotted in Figs. 10 and 11. The solid lines in the figures represent the prediction of the model using the temperature given in literature and assuming the same terrace length as in Figs. 8 and 9. In both cases, the comparison is favorable in light of the fact that we have not introduced any additional fitting parameters to the model. All parameters were determined from fitting the temperature dependence as given in Table IV.

We believe the systematic deviation of the predicted behavior from the experimental data is due to the assumption in the model calculations of a fixed terrace length for all deposition fluxes. Based on the analysis of temperature dependence of segregation of both P and Sb, we place the experiments in the kinetically limited regime of the step-edge-mediated process, regime II. Thus we expect that changes in the terrace length with increasing deposition flux will affect the segregation ratio. If we assume a scaling behavior in which the average terrace length decreases with the nth power of deposition flux,[55] then the magnitude of the slope of the model curves in Figs. 10 and 11 decreases and brings the model curves more in line with the experimental measurements. This is demonstrated by the dashed curves in these figures where we have assumed the relationship $L \propto R^{-1/3}$ (Ref. 56). However, in the absence of any information about the actual terrace lengths in the experimental samples, we view this agreement as encouraging but tentative.

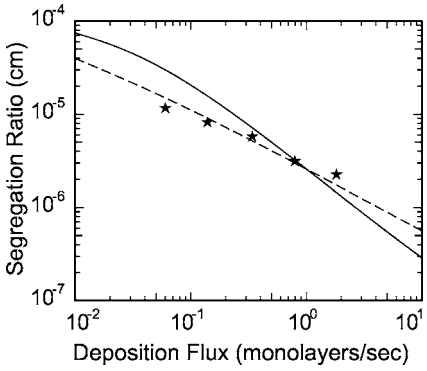

FIG. 11. Fit of deposition-flux-dependent segregation ratio for P in Si(001). The symbols represent experimental data obtained from Ref. 32. Parameters were fixed to those of Table IV. Best fit values were obtained for $1000/T=1.58$. Dashed line represents fit using the same parameters but allowing the terrace length to vary as the deposition rate, $L \propto R^{-1/3}$.

VI. SUMMARY

We have developed a unified kinetic model for segregation that incorporates parallel mechanisms for segregation at the step edge and throughout the terrace. We start with a fundamental description of mass transport, Eqs. (9)–(14), and simplify the system using a reasonable set of assumptions and assertions. The result is an analytic form for the segregation ratio given by Eqs. (39) and (35). The four adjustable parameters in the model represent the segregation energies and activation barriers at the step edge and in the terrace.

The temperature dependence of the segregation ratio exhibits a transition between kinetically limited and equilibrium segregation regimes. Additional temperature regimes are identified, depending on the relative magnitudes of the four energy parameters. The model further predicts the dependence of the segregation ratio on growth rate and miscut angle.

The model readily accounts for the anomalous low-temperature segregation behavior observed for Sb in Si(001) as well as the more typical behavior of P in Si(001). The energies and preexponential factors used in the successful fits, tabulated in Table IV, are consistent with previously reported values. We attribute the low-temperature behavior to the onset, with increasing temperature, of a lower activation energy step-edge-mediated process that becomes overwhelmed by terrace-mediated processes at higher temperatures. The same parameters are used to calculate the growth rate dependence of the segregation ratio without any fitting, resulting in a good agreement with experiment. Additional experiments or first principles calculations are possible to determine the energies independently, thereby permitting a reduction in the number of free fitting parameters needed to model the experimental data.

Although the model has been ostensibly developed to describe experimental results in Si-based systems, the phenomenology and mechanisms are of sufficient generality that they are applicable to other group IV and III-V semiconductors, as well as to segregating metal systems. These analytic results can be used to gain physical insight into the segregation behavior in real systems as well as to account quantitatively for experimental data.

ACKNOWLEDGMENTS

The authors thank I. Berbezier for helpful conversations. Research at Harvard was supported by NSF-DMR-0306997 and at Princeton under internal funding.

APPENDIX A: TREATMENT OF EXTENDED STEP EDGE REGION

We recall the initial set of kinetic equations for the model [Eqs. (9)–(14)] and note the similarity between pairs of equations for T,P and S,E before making the assumption that the step-edge region is limited to a single atomic spacing. Then the generalization to an extended step-edge region is readily accomplished by noting that the steady-state equations for regions S and E [Eqs. (25) and (26)] become identical to those for T and P given in Eqs. (23) and (24) with the appropriate changes in superscript. Under these assumptions, the steady-state solutions for concentration are solved as before to yield

$$\frac{C^S(x)}{C_{bulk}} = \mathbb{A}^S e^{-\kappa' x} + \mathbb{B}^S, \tag{A1}$$

$$\frac{C^T(x)}{C_{bulk}} = \mathbb{A}^T e^{-\kappa x} + \mathbb{B}^T, \tag{A2}$$

$$\frac{C^E(x)}{C_{bulk}} = -\mathbb{A}^S e^{-\kappa' x} + k_e^{SE}\mathbb{B}^S, \tag{A3}$$

$$\frac{C^P(x)}{C_{bulk}} = -\mathbb{A}^T e^{-\kappa x} + k_e^{TP}\mathbb{B}^T. \tag{A4}$$

Equations (A2) and (A4) are identical to Eqs. (30) and (29) from Sec. III C, with

$$\kappa = \frac{v_d^{TP}}{v a_o}(1 + k_e^{TP}), \tag{A5}$$

$$\kappa' = \frac{v_d^{SE}}{v a_o}(1 + k_e^{SE}). \tag{A6}$$

The unknown constants, $\mathbb{A}^S$, $\mathbb{B}^S$, $\mathbb{A}^T$, and $\mathbb{B}^T$, are solved by applying the boundary conditions of concentration continuity between regions,

$$C^S(w) = C^T(w), \tag{A7}$$

$$C^T(L) = C^E(0), \tag{A8}$$

$$C^E(w) = C^P(w), \tag{A9}$$

$$C^S(0) = C_{Bulk}, \tag{A10}$$

where w is the width of the step-edge region. The last boundary condition arises from the fact that $C^{inc} = C_{Bulk}$. We solve this set of simultaneous equations to find

$$\mathbb{A}^S = \frac{e^{-\kappa(L-w)}(k_e^{SE} - k_e^{TP}) - (1 - k_e^{SE}k_e^{TP})}{e^{-\kappa(L-w)}[k_e^{SE} - k_e^{TP} + e^{-\kappa' w}(1 + k_e^{TP})] + k_e^{TP}(1 + k_e^{SE})}, \tag{A11}$$

$$\mathbb{B}^S = \frac{(1 + e^{-\kappa(L-w)-\kappa' w})(1 + k_e^{TP})}{e^{-\kappa(L-w)}[k_e^{SE} - k_e^{TP} + e^{-\kappa' w}(1 + k_e^{TP})] + k_e^{TP}(1 + k_e^{SE})}, \tag{A12}$$

$$\mathbb{A}^T = e^{\kappa w}\frac{e^{-\kappa' w}(1 - k_e^{SE}k_e^{TP}) + (k_e^{SE} - k_e^{TP})}{e^{-\kappa(L-w)}[k_e^{SE} - k_e^{TP} + e^{-\kappa' w}(1 + k_e^{TP})] + k_e^{TP}(1 + k_e^{SE})}, \tag{A13}$$

$$\mathbb{B}^T = \frac{(1 + e^{-\kappa(L-w)-\kappa' w})(1 + k_e^{SE})}{e^{-\kappa(L-w)}[k_e^{SE} - k_e^{TP} + e^{-\kappa' w}(1 + k_e^{TP})] + k_e^{TP}(1 + k_e^{SE})}. \tag{A14}$$

Then the segregation ratio can be determined from the surface excess by Eq. (8). The surface excess is obtained from Eq. (36),

$$\frac{\Gamma}{C_{bulk}} = \frac{a}{L}[w\mathbb{B}^S(1 + k_e^{SE}) + (L - w)\mathbb{B}^T(1 + k_e^{TP})] - 2a. \tag{A15}$$

However, we recognize from Eqs. (A12) and (A14),

$$\mathbb{B}^S = \mathbb{B}^T\frac{1 + k_e^{TP}}{1 + k_e^{SE}}, \tag{A16}$$

which allows us to obtain the segregation ratio,

$$r = a(1 + k_e^{TP})\mathbb{B}^T. \tag{A17}$$

This result is identical to the segregation ratio derived in Eq. (39) with the substitution of $\mathbb{B}^T$ for $\mathbb{B}$.

APPENDIX B: TREATMENT OF ADATOM LAYERS M AND R

In this appendix, we show that sufficient conditions for the adatom region to not contribute significantly to the overall surface excess of Eq. (36) are that the system is dilute everywhere, there are no vertical exchange events between surface and adatom states, and impurity adatoms are energetically unfavorable. Consider the time-dependent concentrations in the regions M and R which are described by Eqs. (13) and (14). Given the assumption that there is no vertical exchange between regions S and M or between T and R, $J^{\alpha\beta}$ is zero and we can rewrite the equations,

$$\frac{\partial C^R}{\partial t} = D^R\frac{\partial^2 C^R}{\partial x^2} - v\frac{\partial C^R}{\partial x} - C^R k^{R,evap} + \frac{fF}{aa_o^2}, \tag{B1}$$

$$\frac{\partial C^M}{\partial t} = D^M\frac{\partial^2 C^M}{\partial x^2} - v\frac{\partial C^M}{\partial x} - C^M k^{M,evap} + \frac{fF}{aa_o^2}. \tag{B2}$$

As both equations are identical except for the superscripts denoting the region, we express the equations with the superscript *ad* to denote the adatom region which can be either M or R. Then the following equations represent the solutions for either M or R depending on the spatial coordinate x. For

$0 \leqslant x < w$, $ad=M$ and $w < x \leqslant L$, $ad=R$. In steady state the differential equations become

$$0 = D^{ad}\frac{d^2C^{ad}}{dx^2} - v\frac{dC^{ad}}{dx} - C^{ad}k^{ad,evap} + \frac{fF}{aa_o^2}. \quad \text{(B3)}$$

This equation is readily solved to give

$$C^{ad}(x) = C_1^{ad}e^{m_1^{ad}x} + C_2^{ad}e^{m_2^{ad}x} + \frac{fF}{aa_o^2}, \quad \text{(B4)}$$

where C_1^{ad} and C_2^{ad} are constants of integration and

$$m_{1,2}^{ad} = \frac{1}{2}\left[\frac{v}{D^{ad}} \pm \sqrt{\left(\frac{v}{D^{ad}}\right)^2 + 4\frac{k^{ad,evap}}{D^{ad}}}\right].$$

The constants of integration are found by applying the appropriate boundary conditions of continuity in both concentration and flux at $x=w$ and no step-climb flux (i.e., R $\rightarrow$M) across the boundary at $x=0$. For the fourth boundary condition, we assume no diffusive flux at the boundary $x=L$. These conditions result in the boundary equations,

$$C^M(w) = C^R(w), \quad \text{(B5)}$$

$$\frac{dC^M}{dx}(w) = \frac{dC^R}{dx}(w), \quad \text{(B6)}$$

$$\frac{dC^M}{dx}(0) = \frac{v}{D^M}C^M(0), \quad \text{(B7)}$$

$$\frac{dC^R}{dx}(L) = 0, \quad \text{(B8)}$$

a discussion of which is deferred to the end of this appendix.

In order to prove the contribution of the adatom region to the segregation length is small in comparison to that of the other regions, we look at the equation for the individual contribution from the adatom region to the segregation ratio,

$$r_{ad} = \frac{\frac{a}{L}\int_0^L C^{ad}(x)dx}{C_{bulk}}. \quad \text{(B9)}$$

Without solving the integral, we can rewrite the equation as

$$r_{ad} = \frac{a\overline{C^{ad}}}{C_{bulk}}, \quad \text{(B10)}$$

where $\overline{C^{ad}}$ is the average value of $C^{ad}(x)$ as defined by the mean value theorem. However, by definition of average value, if $C^{ad}(x)$ is a monotonically increasing function, $C^{ad}(0) < \overline{C^{ad}} < C^{ad}(L)$.

$C^{ad}(L)=C^{inc}$ due to our assumptions and $C^{inc}=C_{bulk}$ because we are in steady state, thus r_{ad} will always be less than a. However, from Secs. IV A and IV B, for all temperatures, $r \geqslant 2a$. Therefore, the contribution of the adatom region to the overall segregation length will be small.

It remains to prove that $C^{ad}(x)$ is a monotonically increasing function. This is done by solving the set of equations using the boundary conditions and taking the first derivative. Because the extent of region M is small relative to R ($w \ll L$, see Appendix A), we include the proof for region R. The proof for region M follows similarly. Solving Eq. (B4) subject to the boundary conditions yields

$$C^R(x) = \mathbb{C}(m_2^R e^{m_2^R L + m_1^R x} - m_1^R e^{m_1^R L + m_2^R x}) + \frac{fF}{aa_o^2}, \quad \text{(B11)}$$

where $\mathbb{C}$ is a positive constant. We take the first derivative and simplify the equation by substituting back in for m_1 and m_2 to obtain

$$\frac{dC^R(x)}{dx} = C\frac{k^{R,evap}}{D^R}\exp\left(\frac{v(L+x)}{2D^R}\right) \times 2\sinh\left(\frac{L-x}{2}\sqrt{\frac{v^2}{(D^R)^2} + \frac{4k^{R,evap}}{D^R}}\right). \quad \text{(B12)}$$

However, for $D < \infty$, all the terms in the above equation are greater than zero so

$$\frac{dC^{ad}(x)}{dx} > 0, \quad \text{(B13)}$$

and hence $C^{ad}(x)$ is a monotonically increasing function.

In defining the boundary conditions [Eqs. (B5)–(B8)] we have assumed that there is no lateral exchange between regions (R) and (S), and no step climbing mechanisms that enable impurity atoms to remain in an adatom state without attaching to a step edge. It is conceivable that arbitrary experimental conditions could yield either or both of these phenomena. Although the kinetic barriers and mechanisms are different, the net result of either is to change the relation between $C^R(L)$ and C^{inc}. In either case, there will be a velocity-dependent partition coefficient[21] that establishes a concentration discontinuity between (R) and (S), ΔC^R, leading to $C^{inc}=C^R(L)-\Delta C^R$.

Our proof remains valid provided $r_{ad} < r$. Therefore, this condition becomes

$$\Delta C^R < \frac{C^R(L)(r-a)}{r}. \quad \text{(B14)}$$

Because $r \geqslant 2a$ for all temperatures, this inequality can be used to find that if $\Delta C^R < C^R(L)/2$, our assertion is valid and regions (M) and (R) may be ignored. Typically, we expect that an impurity atom is more stable energetically in S than in R, in which case ΔC^R should be small enough for this condition to hold. However, there could be systems in which the impurity has such large repulsive interactions with the host that the adatom state is energetically preferred to the step-edge state. This condition could be violated in such systems.

*Electronic address: cbarnold@princeton.edu

[1] E. Schubert, *Delta-Doping of Semiconductors* (Cambridge University Press, Cambridge, 1996).
[2] H. J. Gossmann and E. F. Schubert, Crit. Rev. Solid State Mater. Sci. **18**, 1 (1993).
[3] F. Capasso, Science **235**, 172 (1987).
[4] H. C. Liu and F. Capasso, *Intersubband Transitions in Quantum Wells: Physics and Device Applications II* (Academic, San Diego, CA, 2000).
[5] C. Gmachl, F. Capasso, D. L. Sivco, and A. Y. Cho, Rep. Prog. Phys. **64**, 1533 (2001).
[6] L. Oberbeck, N. J. Curson, M. Y. Simmons, R. Brenner, A. R. Hamilton, S. R. Schonfield, and R. G. Clark, Appl. Phys. Lett. **81**, 3197 (2002).
[7] S. A. Wolf, D. D. Awschalom, R. A. Buhrman, J. M. Daughton, S. VonMonar, M. L. Roukes, A. Y. Chtchelkanova, and D. M. Treger, Science **294**, 1488 (2001).
[8] I. Zutic, J. Fabian, and S. DasSarma, Rev. Mod. Phys. **76**, 323 (2004).
[9] P. B. Allen, Solid State Commun. **102**, 127 (1997).
[10] R. F. C. Farrow, IBM J. Res. Dev. **42**, 43 (1998).
[11] R. Skomski, J. Phys.: Condens. Matter **15**, 841 (2003).
[12] J. F. Bobo, L. Gabillet, and M. Bibes, J. Phys.: Condens. Matter **16**, 471 (2004).
[13] S. Manoharan, J. Shen, H. Jenniches, M. Klaua, and J. Kirschner, J. Appl. Phys. **81**, 3768 (1997).
[14] M. E. Taylor, G. He, C. Saipetch, and H. A. Atwater, in *Film Synthesis and Growth Using Energetic Beams*, edited by H. A. Atwater, J. T. Dickinson, D. H. Lowndes, and A. Polman (Materials Research Society, Pittsburgh, PA, 1995), Vol. 388, pp. 97–103.
[15] R. Kubiak and C. Parry, in *Silicon Molecular Beam Epitaxy*, edited by J. Bean, S. Iyer, and K. Wang (Materials Research Society, Pittsburgh, PA, 1991), Vol. 220, pp. 63–74.
[16] H. J. Gossmann, E. F. Schubert, D. J. Eaglesham, and M. Cerullo, Appl. Phys. Lett. **57**, 2440 (1990).
[17] O. D. Dubon, P. G. Evans, J. F. Chervinsky, M. J. Aziz, F. Spaepen, J. A. Golovchenko, M. F. Chisholm, and D. A. Muller, Appl. Phys. Lett. **78**, 1505 (2001).
[18] A. Portavoce, I. Berbezier, and A. Ronda, Phys. Rev. B **69**, 155416 (2004).
[19] D. J. Eaglesham, H. J. Gossmann, and M. Cerullo, Phys. Rev. Lett. **65**, 1227 (1990).
[20] J. J. Harris, D. E. Ashenford, C. T. Foxon, P. J. Dobson, and B. A. Joyce, Appl. Phys. A: Solids Surf. **A33**, 87 (1984).
[21] M. J. Aziz, J. Appl. Phys. **53**, 1158 (1982).
[22] L. M. Goldman and M. J. Aziz, J. Mater. Res. **2**, 524 (1987).
[23] S. S. Iyer, R. A. Metzger, and F. G. Allen, J. Appl. Phys. **52**, 5608 (1981).
[24] A. Rockett, T. Drummond, J. Greene, and H. Morkoc, J. Appl. Phys. **53**, 7085 (1982).
[25] S. Barnett and J. Greene, Surf. Sci. **151**, 67 (1985).
[26] C. E. C. Wood and B. A. Joyce, J. Appl. Phys. **49**, 4854 (1978).
[27] Models of Barnett *et al.* (Refs. 24 and 25) used this type of formulation. However, its validity was later demonstrated by Tersoff through a kinetic argument based on impurity-induced stress at the free surface [J. Tersoff, Phys. Rev. Lett. **74**, 5080 (1995)].
[28] H. Jorke, Surf. Sci. **193**, 569 (1988).
[29] S. Fukatsu, K. Fujita, H. Yaguchi, Y. Shiraki, and R. Ito, Appl. Phys. Lett. **59**, 2103 (1991).
[30] J. Tsao, *Materials Fundamentals of Molecular Beam Epitaxy* (Academic, Boston, 1993).
[31] S. Andrieu, F. A. d'Avitaya, and J. Pfister, J. Appl. Phys. **65**, 2681 (1989).
[32] J. F. Nutzel and G. Abstreiter, Phys. Rev. B **53**, 13551 (1996).
[33] Y. Y. Hervieu and M. P. Ruzaikin, Surf. Sci. **408**, 57 (1998).
[34] D. E. Jesson, S. J. Pennycook, and J. M. Baribeau, Phys. Rev. Lett. **66**, 750 (1991).
[35] M. Karimi, T. Kaplan, M. Mostoller, and D. E. Jesson, Phys. Rev. B **47**, 9931 (1993).
[36] J. Deppe, J. V. Lill, D. J. Godbey, and K. D. Hobart, in *Compound Semiconductor Epitaxy*, edited by C. Tu, L. Kolodziejski, and V. McCrary (Materials Research Society, Pittsburgh, PA, 1994), Vol. 340, pp. 47–52.
[37] S. Bendi, R. Venkatsubramanian, and D. L. Dorsey, J. Appl. Phys. **76**, 5202 (1994).
[38] J. M. Roussel, A. Saul, G. Treglia, and B. Legrand, Surf. Sci. **352-354**, 562 (1996).
[39] J. A. Floro and E. Chason, Appl. Phys. Lett. **69**, 3830 (1996).
[40] G. Jernigan, P. E. Thompson, and C. L. Silvestre, Appl. Phys. Lett. **69**, 1894 (1996).
[41] D. Kandel and E. Kaxiras, Solid State Phys. **54**, 219 (2000).
[42] In the case of a perfectly flat surface, as in the Jorke formulation, there is no difference between the real surface area and the projected area and no distinction is made. However, as one considers roughened surfaces with step edges, experimental measurements for surface area (such as profiling or desorption techniques) may yield a larger area and subsequently lower 2-D areal concentration if used in the calculations. Throughout the development of our model, we consider only the unambiguous projected surface area and thus experimental comparisons should use a similar calculation.
[43] It is possible that the different deposition cases will result in dissimilar growth morphologies or step densities on the surface for given experimental conditions [for instance, G. G. Jernigan and P. E. Thompson, Thin Solid Films **380**, 114 (2000)]. However, differences in growth morphology are independently taken into account through the terrace length dependence derived in the model.
[44] A related assertion is that lateral exchange (such as $S \rightarrow T$ or $T \rightarrow E$) can be similarly ignored as these do not lead to a net change in the surface concentration. However, such mechanisms can be easily included by either adding an explicit flux in Eqs. (9)–(14) or by modifying the boundary conditions between regions. Other lateral exchanges with the adatom regions (M and R) are related to assertion 3.
[45] C. B. Arnold and M. J. Aziz, in *Growth, Evolution and Properties of Surfaces, Thin Films and Self-Organized Structures*, edited by S. S. Moss (Materials Research Society, Pittsburgh, PA, 2001), Vol. 648, pp. 3.11–3.19.
[46] M. J. Aziz and T. Kaplan, Acta Metall. **36**, 2335 (1988).
[47] If this assumption is reversed, then the equations would have a sign change as previously described by M. J. Aziz and W. J. Boettinger [Acta Metall. Mater. **42**, 527 (1994)]. Such a switch would imply that a B atom has a bias toward bulk rather than toward the surface which is in contrast with the initial assumption that impurity atoms prefer to segregate to the free surface.
[48] By assuming the dilute limit, the model loses the ability to account for self-limiting behavior that may occur with high doping

levels or alloy growth. For impurities that tend to segregate, this assumption is expected to be most restrictive in region S. A full treatment of the nondilute case follows directly from this work but is beyond the scope of the current paper.

[49] J. Nutzel and G. Abstreiter, J. Appl. Phys. **78**, 937 (1995).

[50] M. Ladeveze, F. Bassani, F. A. D'Avitaya, G. Treglia, C. Dubois, and R. Stuck, Phys. Rev. B **56**, 7615 (1997).

[51] H. Jorke, H. J. Herzog, and H. Kibbel, Fresenius' J. Anal. Chem. **341**, 176 (1991).

[52] Z. M. Jiang, C. W. Pei, L. S. Liao, X. F. Zhou, X. J. Zhang, X. Wang, T. Smith, and I. K. Sou, Thin Solid Films **336**, 236 (1998).

[53] K. D. Hobart, D. J. Godbey, M. E. Twigg, M. Fatemi, P. E. Thompson, and D. S. Simons, Surf. Sci. **334**, 29 (1995).

[54] There are data from Jorke's paper (Ref. 28) that are qualitatively consistent in terms of a transition between kinetically limited and equilibrium segregation, but the transition temperature is inconsistent with later work by the same group (see Ref. 51). Therefore we have chosen to ignore the earlier data and consider our fit to be a lower bound on $\Delta\mu^{TP}$.

[55] A. L. Barabasi and H. Stanley, *Fractal Concepts in Surface Growth* (Cambridge University Press, Cambridge, UK, 1995).

[56] R. S. Ross and M. F. Gyure, Phys. Rev. B **61**, 8602 (2000).

[57] L. Oberbeck, N. J. Curson, T. Hallam, M. Y. Simmons, G. Bilger, and R. G. Clark, Appl. Phys. Lett. **85**, 1359 (2004).